Lidar reveals uniform Alpine fault offsets and bimodal plate boundary rupture behavior, New Zealand

Gregory P. De Pascale*, Mark C. Quigley, and Tim R.H. Davies
Department of Geological Sciences, University of Canterbury, Christchurch 8140, New Zealand

ABSTRACT

Analysis of light detection and ranging (lidar) derived topography combined with field data enables measurement of small (<30 m), previously unrecognized dextral offsets beneath dense temperate rainforest along New Zealand's central Alpine fault. Field offset measurements often have lower uncertainties than lidar measurements. Offsets of 7.5 ± 1 m for the most recent earthquake (ca. A.D. 1717) and cumulative offsets of 12.9 ± 2 m and 22 ± 2.7 m can be averaged into three 7.1 ± 2.1 m increments of repeated dextral slip at a point, and when combined with an offset compilation show a uniform slip distribution of ~7.5 ± 2.0 m over 300 km in A.D. 1717. Comparing these offsets with the 1.1 ka paleoseismic record and slip rate demonstrates a mismatch between offsets, timing, and slip rate that can be explained in two ways: (1) major (full) ruptures (moment magnitude, M_w ≥7.9) every 270 ± 70 yr (e.g., A.D. 1717) and with moderate to large (partial rupture) Alpine fault earthquakes (M_w ≥6.5; e.g., A.D. 1600) occurring between full ruptures, and (2) some off-fault shaking data may instead reflect paleoseismicity from other faults. If explanation 1 is true, the Alpine fault has two (i.e., bimodal) or more modes of behavior (or the slip rate has not been constant since 1.1 ka) and rupture is perhaps width limited. If explanation 2 is true, perhaps the Alpine fault behavior is characteristic, and other faults are responsible for some shaking records. Ultimately, bimodal behavior is our preferred interpretation, which has implications for our understanding of plate boundary seismic hazards worldwide.

INTRODUCTION

Understanding the behavior of plate boundary faults and the recurrence of major earthquakes along these faults is critical for understanding seismic hazards. Displaced surface features along the Alpine fault (AF), the dextral-reverse plate boundary structure with ~480 km of dextrally offset bedrock terranes between the Pacific and Australian plates on the South Island of New Zealand (Fig. 1; Wellman, 1953; De Mets et al., 2010), provide an opportunity to investigate its earthquake history and provide insight into plate boundary behavior. The most recent surface rupture along the AF (i.e., most recent event) was a great earthquake (estimated moment magnitude, M_w, of 8.1 ± 0.1; Wells et al., 1999; De Pascale and Langridge, 2012) in A.D. 1717 (Fig. 1) that had an onshore rupture length of at least 380 km (Wells et al., 1999). Slip during the most recent event and previous events were hitherto unknown, due largely to the high rainfall, rugged topography, and dense temperate rainforest cover that hinder investigations. To investigate the rupture behavior of the AF, we mapped offsets along the central AF using light detection and ranging (lidar) data and field investigations that we compared with other AF earthquake evidence.

The ~200-km-long central AF (Fig. 1) extends from near Haast to the Kokatahi River, and bounds the western edge of the Southern Alps (Norris and Cooper, 2001). This section of the fault is characterized by strike-slip rates (27 ± 5 mm/yr) and dip-slip rates (8–12 mm/yr) determined from geological observations (Norris and Cooper, 2001), and represent 50%–80% of the 39.7 ± 0.7 mm/yr relative motion across the plate boundary (Sutherland et al., 2007; De Mets et al., 2010). Microseismicity and geodetic studies demonstrate that the central AF is currently locked and without earthquakes of M_w > 2.5 (e.g., Wallace et al., 2007; Boese et al., 2012).

The timing of AF earthquakes is inferred because the fault has not ruptured during New Zealand's short (since A.D. 1840) post-European colonization period (Fig. 1). On-fault AF investigations use direct evidence of rupture such as displaced geologic or geomorphic features (Wells et al., 1999; Langridge et al., 2010; Berryman et al., 2012a; De Pascale and Langridge, 2012), whereas off-fault shaking records may be

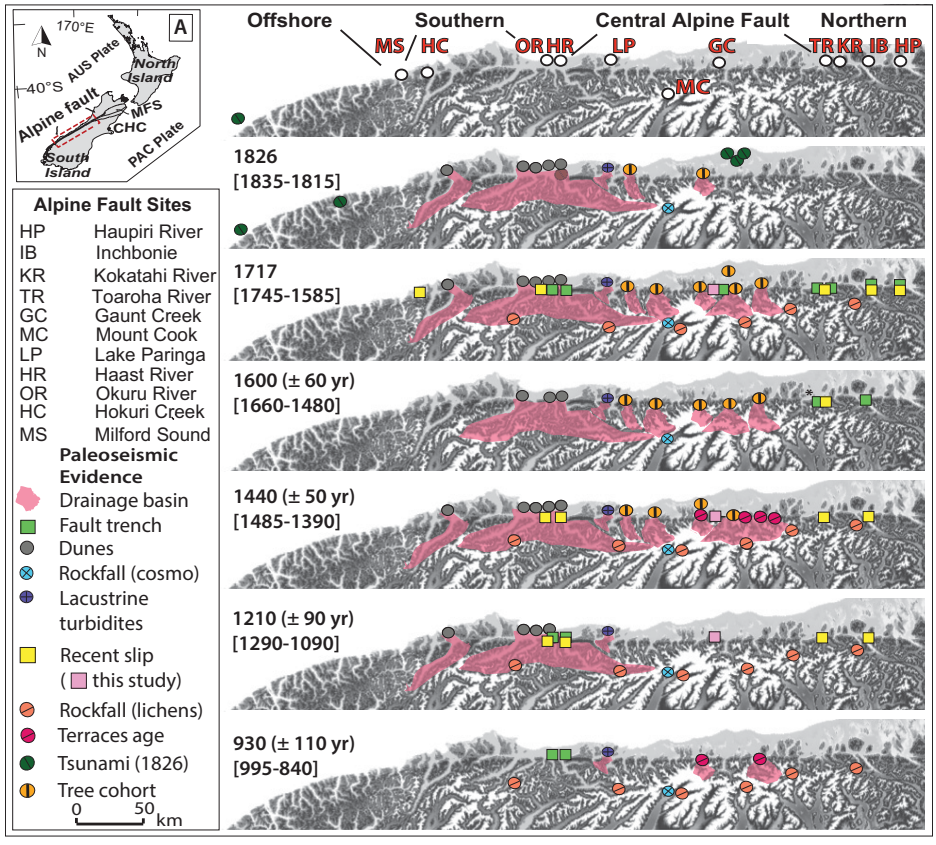

Figure 1. Inset A: Map of New Zealand showing Marlborough fault system (MFS), Alpine fault (AF), Christchurch (CHC), and Pacific (PAC) and Australian (AUS) plates. Main map: Type (boxes represent on-fault data), timing, and locations of on-fault and off-fault (shaking) paleoseismic data for past 1.1 k.y. along AF. Note data coincident with slip estimates from this study in A.D. 1717, ca. 1440, and ca. 1210.

*Current address: Fugro Geotechnical (NZ), Middleton, Christchurch 8024, New Zealand; E-mail: snowyknight@gmail.com.

<1 km to hundreds of kilometers from a fault, and provide evidence for strong ground motions at or upstream of a site (Fig. 1; note the affected drainage basins). AF shaking records include dating of coseismic rock falls and landslides (Bull, 1996; Reznichenko et al., 2012), post-earthquake aggradational terraces (Adams, 1980), tree rings (Wells et al., 1999), deformed river terraces, buried surfaces and trees (Adams, 1980; Wells et al., 1999), coastal dune progradation sequences (Wells and Goff, 2007), lacustrine megaturbitides (Howarth et al., 2012), and varved sedimentary sequences (Berryman et al., 2012b). Combined records unambiguously show the most recent event in 1717 (Fig. 1), with on-fault evidence for ruptures at ca. 1600 (Wells et al., 1999), ca. 1210, and ca. 930 (Berryman et al., 2012a). Off-fault records indicate strong shaking at ca. 1826, 1717, 1600, 1440, 1210, and 930 (Adams, 1980; Bull, 1996; Wells et al., 1999; Wells and Goff, 2007; Reznichenko et al., 2012; Howarth et al., 2012; Berryman et al., 2012b). Sutherland et al. (2007) suggested that the 1717, 1600, and 1400 events had noncharacteristic behavior, with variable magnitudes and rupture lengths. Recent studies argue for 260 ± 70 yr to 480 yr (Howarth et al., 2012; Berryman et al., 2012a) intervals between major AF earthquakes; Berryman et al. (2012b) obtained a recurrence interval of 329 ± 68 yr over 8 k.y.

Creeks and fluvial landforms that cross strike-slip faults provide important piercing points, and enable estimates of slip (e.g., Wallace, 1968; Sieh, 1978; McGill and Sieh, 1991). The smallest offset measured along a fault is conventionally attributed to the most recent event, with larger values representing cumulative offsets. High-resolution topographic data (e.g., Arrowsmith and Zielke, 2009; Zielke et al., 2010; Salisbury et al., 2012) demonstrate that remote and reproducible offset measurements are possible where vegetation is sparse. Known small-offset measurements are rare along the entire AF (Figs. 1 and 2); only eight offset locations were reported prior to this study (Berryman, 1975; Sutherland and Norris, 1995; Wells et al., 1999; Langridge et al., 2010; Berryman et al., 2012a, 2012b).

METHODS

Remote sensing and field mapping were used to detect and measure offsets along the central AF (see the GSA Data Repository[1]). A 34-km-long, 1-km-wide swath of airborne lidar data (see Langridge et al., 2013) allowed the generation of a 2 m digital elevation model (DEM). The DEM was imported into ArcGIS (http://www.esri.com/software/arcgis), where hillshade, slopeshade, and topographic maps were used to delineate and measure displaced geomorphic features (<30 m; Fig. 3) and to identify linear valleys, sag ponds, thalwegs of small channels, channel margins, and wind gaps that demarcate AF rupture traces. The abundance of rainfall (5–15 m/yr), and dynamic nature of the landscape support the assumption that most fluvial features form between major earthquakes and are then offset by the next earthquake, giving a clear record of progressive ruptures (e.g., Wallace, 1968; Grant Ludwig et al., 2010). We identified offset fault-perpendicular features at seven new sites along the fault and projected them into the fault using a variety of angles reflecting our uncertainties (including postevent erosion of features), and measured these offsets. We report a central preferred measurement together with minimum and maximum measurements (e.g., McGill and Sieh, 1991). The largest difference between the preferred value and accepted minimum or maximum value was used to assign the uncertainty to the ideal displacement measurement (e.g., Zielke et al., 2010; Salisbury et al., 2012). These sites were then back-slipped (e.g., Zielke et al., 2010) in order to check the preferred offset amounts (Fig. 3). Field validation of remote mapping along the AF is difficult; however, we located these same displacements in the field, often using creek channels to ex-

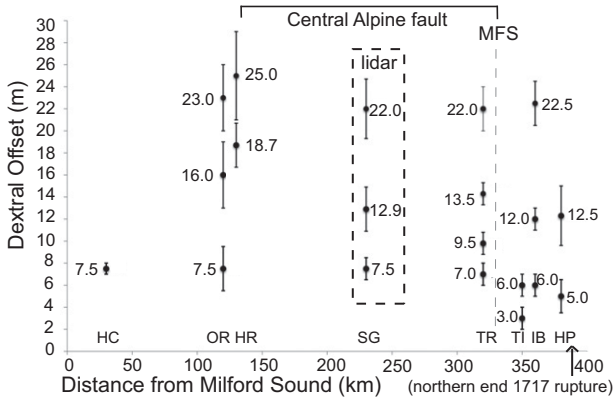

Figure 2. Compilation of offsets along Alpine fault (AF), New Zealand. HC—Hokuri Creek, OR—Okuru River, HR—Haast River, SG—South of Gaunt Creek, TR—Toaroha River, TI—Taipo River, IB—Inchbonnie, HP—Haupiri River (southwest to northeast). SG offsets are new (this study). Marlborough fault system (MFS) intersections with AF northern termination of A.D. 1717 rupture are noted.

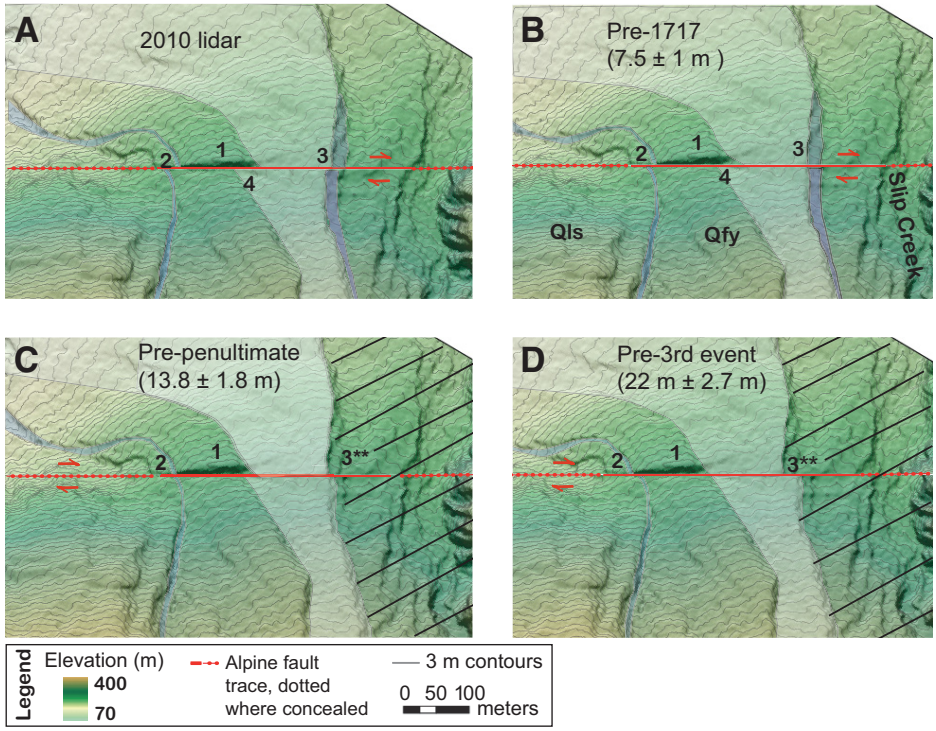

Figure 3. Lidar hillshade of sites south of Gaunt Creek (New Zealand, 43°19′19.28″S, 170°18′35.57″E), with back-slipping to restore landforms. A: Post–A.D. 1717 (2010 lidar digital elevation model). B: Prior to most recent event with 7.5 ± 1 m dextral back-slip at channel margin (3). C: Prior to penultimate event with 13.75 ± 1.8 m back-slip at wind gap (2). D: Prior to third-oldest event with 22 ± 2.7 m of slip at shutter ridge (1). Note that channel margins (3) are crossed; they likely formed after penultimate event. Qls and Qfy represent Quaternary landslides and fans, respectively.**

[1]GSA Data Repository item 2014148, additional methods, site descriptions, maps, and field photos, is available online at www.geosociety.org/pubs/ft2014.htm, or on request from editing@geosociety.org or Documents Secretary, GSA, P.O. Box 9140, Boulder, CO 80301, USA.

Figure 4. Field photograph showing geologist wearing a high-visibility vest while mapping an offset in dense rainforest along the Central Alpine fault, New Zealand.

TABLE 1. DEXTRAL SLIP ALONG THE CENTRAL ALPINE FAULT

Type and timing of slip data	Combined dextral slip with uncertainty (m)	Mean slip with uncertainty (m)	Event timing estimate (yr A.D.)
Combined lidar and field 1717 MRE preferred (n = 2)	7.5 ± 1	7.5 ± 1	1717
Combined lidar and field two events preferred (n = 2)	12.9 ± 2	6.5 ± 2	1430 (±65 yr)
Combined lidar and field three events preferred (n = 1)	22 ± 2.7	7.3 ± 2.7	1180 (±110 yr)
Mean slip averaged over two events	N.A.	7.0 ± 1.7	N.A.
Mean slip averaged over three events	N.A.	7.1 ± 2.1	N.A.

Note: MRE—most recent event. The n values reported refer to individual slip sites, and not number of measurements at these locations. N.A.—not applicable. Summary of combined lidar and field slip data and associated event timing estimates based on a 27 ± 5 mm/yr dextral slip rate (Norris and Cooper, 2001) and assuming the regular recurrence of large, surface-rupturing earthquakes.

pedite access with a handheld GPS (and offset locations preprogramed in as waypoints) and lidar-derived maps, and measured offsets with a tape and compass on the ground (Fig. 4). Both lidar and field measurements were ranked on quality of data (high, medium, low, and poor; after Sieh, 1978), with low- and poor-ranked data excluded from offset calculations. In some cases the field measurements have less uncertainty than the lidar measurements, which were limited to ≥2 m resolution, and here we use field values. South of Gaunt Creek where progressive displacement is apparent (Figs. 1 and 3), a combined uncertainty of ±1 m for the smallest dextral strike-slip displacements was determined based on field observations. We also compiled and mapped published AF offset (Fig. 2) and paleoseismic records (Fig. 1) including uncertainties. Finally, the new dextral offset values (including uncertainties) were divided by the central AF dextral slip rate (27 ± 5 mm/yr; Norris and Cooper, 2001) to explore the timing of past AF ruptures, assuming steady interseismic strain accumulation that is accommodated primarily by slip in large earthquakes (Wallace et al., 2007; Boese et al., 2012).

RESULTS

Our data show a mean value of 7.5 ± 1 m of central AF dextral slip for the smallest offsets, with clusters of larger (cumulative) offsets measured within the lidar swath area averaging 12.9 ± 2 m, and 22 ± 2.7 m (Table 1; Fig. 2; see the Data Repository). In addition, we estimate an average dextral slip of 6.5 ± 2 m for the penultimate (pre-1717 earthquake) and 7.3 ± 2.7 m for the preceding (third) event, collectively defining a mean slip of 7.1 ± 2.1 m for the three events. At Gaunt Creek (Fig. 1), on-fault dating shows that the most recent event along the central AF was the 1717 earthquake (De Pascale and Langridge, 2012); this is supported by abundant shaking records (e.g., Wells et al., 1999; Howarth et al., 2012). We assume that the smallest observed offsets formed coseismically in 1717, although these could have formed in more than one event (e.g., Akciz et al., 2010). After an earthquake, increased landslide debris and base-level change cause aggradation on the steep lower range front fans, with incision of new (and unfaulted) risers forming as the creeks regrade. Offset risers are thus abandoned, preserving offsets via the mechanisms described by Cowgill (2007). Data resolution limited detectability, and therefore only offsets >2 m could be detected in the topographic data; however, in the field smaller offsets (e.g., <2 m to 6.5 m) should be visible on the ground where vegetation density allows, although none were found during field work. Based on the uncertainties in our data and challenging field conditions, offsets smaller than 6.5 m could exist (and thus we may be missing events); however, we find no field or lidar-derived evidence for incremental dextral slip <6.5 m (Table 1; Table DR1; see the Data Repository). Vertical offsets of 0.75 ± 0.25 m, 1.5 ± 0.25 m, and 2.5 ± 1 m were measured in the field south of the Gaunt Creek sites showing progressive slip (Fig. 3), suggesting repeating incremental vertical displacements of ~0.8 m. By dividing the slip by the slip rate, we estimate the timing of pre-1717 central AF earthquakes as ca. 1430 (±65 yr), and 1180 (±110 yr); these are consistent with other records (Fig. 1).

DISCUSSION AND CONCLUSIONS

Central AF dextral slip distribution shows characteristic slip at a point, suggesting that events along this section of the plate boundary are not variable. Small dextral offsets (<10 m) reported from the southern AF (Sutherland and Norris, 1995; Berryman et al., 2012a, 2012b) are within error of our mean central AF estimates, and we interpret this to reflect uniform slip distribution (i.e., 7.5 ± 2 m) sustained along a surface rupture ≥300 km in 1717 (Figs. 1 and 2). North of the Toaroha River (Wells et al., 1999), the smallest offsets are smaller than all southern sites, although one offset there (9.5 m) perhaps records cumulative slip from two or more events. Northern AF sites (Wells et al., 1999; Langridge et al., 2010) are within error of our central AF cumulative offsets where the AF slip rate is reduced due to slip partitioning (e.g., Norris and Cooper, 2001).

Applying the mean 7.1 ± 2.1 m of slip (Fig. 2) to each central AF earthquake in the paleoseismic record (Fig. 1; e.g., 1717, 1600, 1430, and 1180) requires the dextral slip rate in the past ~800 yr along the central AF to be >40 mm/yr. This exceeds by ~10 mm/yr the geodetic (e.g., Wallace et al., 2007) and geologic (Norris and Cooper, 2001) slip rates. These unreasonably high strain release rates can be explained in two ways.

1. Moderate to large partial ruptures of the AF ($M_w \geq 6.5$; although not observed in the seismicity; e.g., Boese et al., 2012) found in trenches with perhaps small surface offsets (<3 m) and in associated shaking records (e.g., 1600; Figs. 1 and 2) may occur between major (>300 km) full AF ruptures ($M_w \geq 7.9$), but the partial ruptures may not contribute substantially to offsets along the central AF (and perhaps are difficult to find), so the offset records remain dominated by major surface ruptures (e.g., Wesnousky, 1994; Zielke and Arrowsmith, 2008; Akciz et al., 2010; Zielke et al., 2010;), or the slip rate has varied since 1.1 ka.

2. Some of the paleoseismic events formerly attributed to the AF actually occurred along other faults (Fig. 1; e.g., the 1826 subduction earthquake; Wells and Goff, 2007).

Ultimately, option 1 indicates bimodal rupture behavior of the AF (perhaps width limited; e.g., Zielke and Arrowsmith, 2008) with insufficient data to address slip rate variability, while option 2 breaks with the common assumption that all seismicity near the plate boundary results from AF ruptures, and perhaps helps explain why shaking (Wells and Goff, 2007; Howarth et al., 2012) and trenching records (Berryman et al., 2012a) near Haast are inconsistent.

Lidar data were invaluable for discovering small (<30 m) dextral offsets under dense temperate rainforest (Fig. 4) along the plate boundary AF, and field work targeting these offsets provided important insight into plate boundary rupture patterns. By attempting to reconcile these offsets with our new AF paleoseismic compilation, we can attempt to better understand slip-release patterns. Recent evidence

from along the San Andreas fault (e.g., Akciz et al., 2010; Grant Ludwig et al., 2010; Zielke et al., 2010; Streig et al., 2014) suggests that existing models (e.g., characteristic earthquake model; Schwartz and Coppersmith, 1984) do not best describe plate boundary fault behavior, and instead, bimodal rupture behavior (with partial and full ruptures; Zielke and Arrowsmith, 2008), or perhaps more than two modes (e.g., variable rupture behavior), is more accurate. Based on our comparison of uniform offsets at a point with the paleoseismic record, there is evidence for bimodal behavior of the AF; this further supports the hypothesis that perhaps plate boundary faults may not be as simple (i.e., characteristic) as proposed by early models. If this is the case, it implies increased frequency of large AF earthquakes (i.e., increased hazard). Additional coordinated on-fault dating and lidar mapping may help to further refine these models. Ultimately, because neither the AF nor the San Andreas fault are isolated plate boundary faults (both have fast-slipping, seismogenic faults nearby; e.g., the Marlborough fault system and the Hayward fault), our second possible interpretation, wherein off-fault records should only cautiously be attributed to specific faults, should not be overlooked in future studies. Combined, these new findings have global implications related to our understanding of major plate boundary fault behavior and associated strong ground motion–related geohazards.

ACKNOWLEDGMENTS

De Pascale was supported by University of Canterbury's Mason Trust & Hari-Hari Field Station, an Education New Zealand International Doctoral Research Scholarship, and a Wellman Research Award by the New Zealand Geoscience Society. Partial funding was from the New Zealand Earthquake Commission. Rob Langridge made major contributions to the lidar collection and discussions. We thank Ursula Cochran, Trevor Hamilton, Mike Oskin, Julie Rowland, and Tim Stahl for comments on this paper. Sinan Akciz and Ozgur Kozaci provided insight into fault behavior. We greatly appreciate reviews by Ramon Arrowsmith, Colin Amos, two anonymous reviewers, and editor James Spotila.

REFERENCES CITED

Adams, J., 1980, Paleoseismicity of the Alpine fault seismic gap, New Zealand: Geology, v. 8, p. 72–75, doi:10.1130/0091-7613(1980)8<72:POTAFS >2.0.CO;2.

Akciz, S.O., Grant Ludwig, L., Arrowsmith, J.R., and Zielke, O., 2010, Century-long average time intervals between earthquake ruptures of the San Andreas fault in the Carrizo Plain, California: Geology, v. 38, p. 787–790, doi:10.1130/G30995.1.

Arrowsmith, J.R., and Zielke, O., 2009, Tectonic geomorphology of the San Andreas fault zone from high resolution topography: An example from the Cholame segment: Geomorphology, v. 113, p. 70–81, doi:10.1016/j.geomorph.2009.01.002.

Berryman, K.R., 1975, Earth deformation studies reconnaissance of the Alpine fault, immediate report, Earth Deformation Section No. 30: Wellington, New Zealand Geological Survey Department of Scientific and Industrial Research, 26 p.

Berryman, K., Cooper, A., Norris, N., Villamor, P., Sutherland, R., Wright, T., Schermer, E., Langridge, R., and Baisi, G., 2012a, Late Holocene rupture history of the Alpine fault in South Westland, New Zealand: Seismological Society of America Bulletin, v. 102, p. 620–638, doi:10.1785/0120110177.

Berryman, K.R., Cochran, U.A., Clark, K.J., Biasi, G.P., Langridge, R.M., and Villamor, P., 2012b, Twenty-four surface-rupturing earthquakes over 8000 years on the Alpine fault, New Zealand: Science, v. 336, p. 1690–1693, doi:10.1126/science.1218959.

Boese, C.M., Townend, J., Smith, E., and Stern, T., 2012, Microseismicity and stress in the vicinity of the Alpine Fault, central Southern Alps, New Zealand: Journal of Geophysical Research, v. 117, B02302, doi:10.1029/2011JB008460.

Bull, W.B., 1996, Prehistorical earthquakes on the Alpine fault, New Zealand: Journal of Geophysical Research, v. 101, p. 6037–6050, doi:10.1029/95JB03062.

Cowgill, E., 2007, Impact of riser reconstructions on estimation of secular variation in rates of strike-slip faulting: Revisiting the Cherchen River site along the Altyn Tagh fault, NW China: Earth and Planetary Science Letters, v. 254, p. 239–255, doi:10.1016/j.epsl.2006.09.015.

DeMets, C., Gordon, R.G., and Argus, D.F., 2010, Geologically current plate motions: Geophysical Journal International, v. 181, p. 1–80, doi:10.1111/j.1365-246X.2009.04491.x.

De Pascale, G.P., and Langridge, R.M., 2012, New on-fault evidence for a great earthquake in A.D. 1717, central Alpine fault, New Zealand: Geology, v. 40, p. 791–794, doi:10.1130/G33363.1.

Grant Ludwig, L., Akçiz, S.O., Noriega, G.R., Zielke, O., and Arrowsmith, J.R., 2010, Climate-modulated channel incision and rupture history of the San Andreas fault in the Carrizo Plain: Science, v. 327, p. 1117–1119, doi:10.1126/science.1182837.

Howarth, J.D., Fitzsimmons, S.J., Norris, R.J., and Jacobsen, G.E., 2012, Lake sediments record cycles of sediment flux driven by large earthquakes on the Alpine fault, New Zealand: Geology, v. 40, p. 1091–1094, doi:10.1130/G33486.1.

Langridge, R.M., Villamor, P., Basili, R., Almond, P., Martinez-Diaz, J.J., and Canora, C., 2010, Revised slip rates for the Alpine fault at Inchbonnie: Implications for plate boundary kinematics of South Island, New Zealand: Lithosphere, v. 2, p. 139–152, doi:10.1130/L88.1.

Langridge, R.M., Ries, W.F., Farrier, T., Barth, N.C., Khajavi, N., and De Pascale, G.P., 2013, Developing sub-5 m LIDAR DEMs for forested sections of the Alpine and Hope faults, South Island, New Zealand: Implications for structural interpretations: Journal of Structural Geology, doi:10.1016/ j.jsg.2013.11.007.

McGill, S.F., and Sieh, K.E., 1991, Surficial offsets on the central and eastern Garlock fault associated with prehistoric earthquakes: Journal of Geophysical Research, v. 96, p. 21597–21621, doi:10.1029/91JB02030.

Norris, R.J., and Cooper, A.F., 2001, Late Quaternary slip rates and slip partitioning on the Alpine fault, New Zealand: Journal of Structural Geology, v. 23, p. 507–520, doi:10.1016/S0191-8141(00)00122-X.

Reznichenko, N.V., Davies, T.R.H., Shulmeister, J., and Larson, S.H., 2012, A new technique for identifying rock avalanche–sourced sediment in moraines and some paleoclimatic implications: Geology, v. 40, p. 319–322, doi:10.1130/G32684.1.

Salisbury, J.B., Rockwell, T.K., Middleton, T.J., and Hudnut, K.W., 2012, LiDAR and field observations of slip distribution for the most recent surface ruptures along the central San Jacinto fault: Seismological Society of America Bulletin, v. 102, p. 598–619, doi:10.1785/0120110068.

Schwartz, D., and Coppersmith, K., 1984, Fault behavior and characteristic earthquakes: Examples from the Wasatch and San Andreas fault zones: Journal of Geophysical Research, v. 89, no. B7, p. 5681–5698, doi:10.1029/JB089iB07p05681.

Sieh, K.E., 1978, Slip along the San Andreas fault associated with the great 1857 earthquake: Seismological Society of America Bulletin, v. 68, p. 1421–1448.

Streig, A.R., Dawson, T.E., and Weldon, R.J., 2014, Paleoseismic evidence of the 1890 and 1838 earthquakes on the Santa Cruz Mountains section of the San Andreas fault, near Corralitos, California: Seismological Society of America Bulletin, v. 104, doi:10.1785/0120130009.

Sutherland, R., and Norris, R.J., 1995, Late Quaternary displacement rate, paleoseismicity, and geomorphic evolution of the Alpine fault: Evidence from Hokuri Creek, South Westland, New Zealand: New Zealand Journal of Geology and Geophysics, v. 38, p. 419–430, doi:10.1080/00288306.1995.9514669.

Sutherland, R., and 18 others, 2007, Do great earthquakes occur on the Alpine fault in central South Island, New Zealand?, *in* Okaya, D., et al., eds., A continental plate boundary: Tectonics at South Island, New Zealand: American Geophysical Union Geophysical Monograph 175, p. 235–251, doi:10.1029/175GM12.

Wallace, L.M., Beavan, J., McCaffrey, R., Berryman, K., and Denys, P., 2007, Balancing the plate motion budget in the South Island, New Zealand using GPS, geological and seismological data: Geophysical Journal International, v. 168, p. 332–352, doi:10.1111/j.1365-246X.2006.03183.x.

Wallace, R.E., 1968, Notes on stream channels offset by the San Andreas fault, southern Coast Ranges, California, *in* Dickinson, W.R., and Grantz, A., eds., Proceedings of the Conference on Geologic Problems of the San Andreas Fault System: Stanford University Publications in the Geological Sciences, v. 11, p. 6–21.

Wellman, H.W., 1953, Data for the study of recent and late Pleistocene faulting in the South Island of New Zealand: New Zealand Journal of Science and Technology, v. 34B, p. 270–288.

Wells, A., and Goff, J., 2007, Coastal dunes in Westland, New Zealand, provide a record of paleoseismic activity on the Alpine fault: Geology, v. 35, p. 731–734, doi:10.1130/G23554A.1.

Wells, A., Yetton, M.D., Duncan, R.P., and Stewart, G.H., 1999, Prehistoric dates of the most recent Alpine fault earthquakes, New Zealand: Geology, v. 27, p. 995–998, doi:10.1130/0091-7613(1999)027<0995:PDOTMR>2.3.CO;2.

Wesnousky, S.G., 1994, The Gutenburg-Richter or characteristic earthquake distribution, which is it?: Seismological Society of America Bulletin, v. 84, p. 1940–1959.

Zielke, O., and Arrowsmith, J.R., 2008, Depth variation of coseismic stress drop explains bimodal earthquake magnitude-frequency distribution: Geophysical Research Letters, v. 35, L24301, doi:10.1029/2008GL036249.

Zielke, O., Arrowsmith, J.R., Ludwig, L.G., and Akciz, S.O., 2010, Slip in the 1857 and earlier large earthquakes along the Carrizo Plain, San Andreas fault: Science, v. 327, p. 1119–1122, doi:10.1126/science.1182781.

Manuscript received 9 September 2013
Revised manuscript received 12 February 2014
Manuscript accepted 17 February 2014

Printed in USA